ACS Catalysis

Research Article

pubs.acs.org/acscatalysis

Titanium–Germoxy Precursor Route to Germanium-Modified Epoxidation Catalysts with Enhanced Activity

Paul J. Cordeiro,[†,§] Pascal Guillo,[§,‡] Charles S. Spanjers,[∥] Ji Woong Chang,[∥] Mike I. Lipschutz,[‡] Meg E. Fasulo,[‡] Robert M. Rioux,[∥] and T. Don Tilley*[,§,‡]

[†]Department of Chemical and Biomolecular Engineering, University of California, Berkeley, Berkeley, California 94720, United States

[‡]Department of Chemistry, University of California, Berkeley, Berkeley, California 94720, United States

[§]Chemical Sciences Division, Lawrence Berkeley National Laboratory, 1 Cyclotron Road, Berkeley, California 94720, United States

[∥]Department of Chemical Engineering, The Pennsylvania State University, University Park, Pennsylvania 16802, United States

Supporting Information

ABSTRACT: The complex $Ti[OGe^iPr_3]_4$ (**1**), prepared via the reaction of $Ti(O^iPr)_4$ with $^iPr_3GeOH$, represents a useful structural and spectroscopic model for titanium–germanium species dispersed onto silica. This precursor was used to introduce site-isolated Ti(IV) centers onto the surface of a mesoporous SBA15 support via the thermolytic molecular precursor method. The local environments of the supported materials (**$TiGe_3SBA15$** and calcined **$TiGe_3SBA15\text{-}O_2$**) were studied by various spectroscopic methods, including X-ray absorption spectroscopy. These materials are active catalysts for the epoxidation of cyclic and terminal olefins with alkyl hydroperoxides under anhydrous conditions. Compared to catalysts synthesized from siloxide-only precursors, the new catalysts produce 2–3 times more product after 9 h under identical reaction conditions for the epoxidations of cyclohexene and 1-octene. The new materials did not significantly leach under reaction conditions.

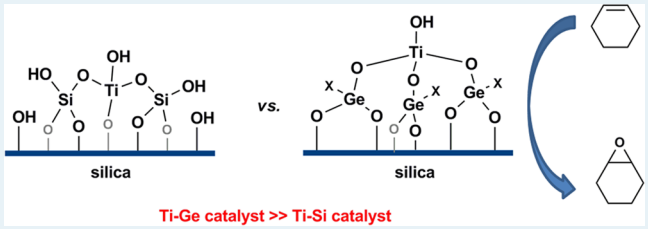

KEYWORDS: *titanium, germanium, site-isolated catalysts, SBA15, epoxidation*

INTRODUCTION

Considerable research in the field of heterogeneous catalysis involves the design, synthesis, and characterization of stable and highly active catalytic sites. Advances in this direction rely on the establishment of structure–activity relationships via mechanistic studies and structural characterization, which are complicated by the inherent difficulty of observing working catalysts under reaction conditions.[1,2] Another significant challenge is the heterogeneity of the active sites that makes characterization and unambiguous determination of catalytic structures difficult to impossible. Many highly active catalysts contain well-defined active sites comprised of one to several metal species, which are directly associated with the observed reactivity. Thus, synthetic methods that allow introduction of precisely controlled metal species are of great interest.

A well-established method for the preparation of isolated, single-site transition-metal catalysts is based on the thermolytic molecular precursor (TMP) method that employs oxygen-rich metal precursor complexes to deliver isolated active sites onto mesoporous supports under mild conditions [illustrated for a silica-supported, single-metal site (Scheme 1)].[3] In this approach, the precursor molecules react with surface silanol (Si-OH) groups and anchor the metal center to the surface. The resulting materials may then be treated in oxygen at mild temperatures (<500 K) to generate metal oxide or hydroxide species, which can then be further functionalized. Various modifications of these surface-bound metal species with groups designed to influence the local coordination environment or the electronic properties of the metal center have been explored. A simple way to accomplish such functionalization involves use of a reagent (e.g., a protic alcohol, ROH in Scheme 1, or amine species) that indiscriminately modifies all -OH groups on the surface, including those of the catalytic center as well as additional sites on the support material.[4−9] A potentially more selective approach involves the "site-directed" incorporation of a new functionality into a suitable metal-containing precursor molecule.

The investigation described below was motivated by the work of Oldryod and co-workers, who observed dramatic enhancements of the catalytic activity of heterogeneous titanium(IV) olefin epoxidation catalysts modified with germanium.[10,11] While only 7% of the catalytic sites possessed a Ti–O–Ge linkage, a 15% enhancement of the catalytic activity was observed. Since this initial report, other catalysts incorporating germanium have been synthesized and applied to a variety of catalytic oxidation reactions.[12−15] More recent theoretical calculations have begun to probe the effect of the germanium atom on the active species in titanium epoxidation catalysts.[14] Liu and co-workers suggested

Received: July 8, 2013
Revised: August 22, 2013
Published: September 13, 2013

   dx.doi.org/10.1021/cs400529x | ACS Catal. 2013, 3, 2269–2279

Scheme 1. Generalized Methodology for the Introduction of Well-Defined, Single-Site Metal Centers via the Thermolytic Molecular Precursor Method

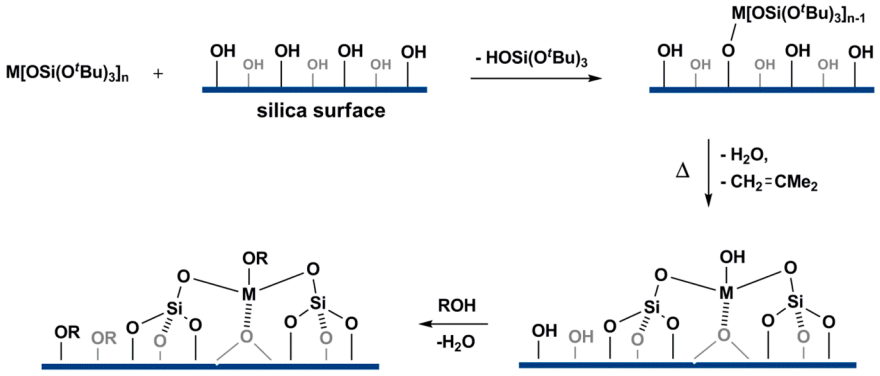

that the proximity of germanium to the titanium center enhances the electrophilicity of the peroxo oxygen atoms in the hydroperoxy intermediate [Ti(η^2-OOH)], thus facilitating the transfer of the electrophilic oxygen to olefins. In related investigations, we described the use of surface functionalization methods[4−7] for the introduction of germanium-containing species into the coordination sphere of silica-supported tantalum(V) olefin epoxidation catalysts.[8] These catalysts demonstrated markedly increased activity with a minimal loss of epoxidation selectivity compared to the related, unmodified catalysts. However, the synthesis of these catalysts involves several steps and results in the nonselective incorporation of germanium onto the support surface. Thus, new catalyst synthesis methods that allow for more controlled and directed introduction of germanium are of interest.

Here we report the synthesis and characterization of a new molecular precursor, Ti[OGe^{i}Pr$_3$]$_4$ (**1**), and its grafting onto mesoporous silica (SBA15) to produce isolated, catalytically active Ti(IV) centers. In comparison to previously described titanium epoxidation catalysts modified by germanium, the catalysts reported here feature a high percentage of titanium centers with a Ti−O−Ge linkage. The resulting supported catalysts were characterized by different solid-state techniques, including X-ray absorption spectroscopy (XAS), and their performance in the epoxidation of cyclohexene and 1-octene using both anhydrous *tert*-butyl hydroperoxide and cumene hydroperoxide was studied. These catalysts are significantly more active than analogous catalysts synthesized from precursors with silicon-based ligands.

RESULTS

Synthesis and Characterization of Ti[OGe^{i}Pr$_3$]$_4$ (1). Initial attempts to synthesize a titanium−germanium precursor compound targeted the germoxy analogue of the previously investigated Ti[OSi(O^{t}Bu)$_3$]$_4$.[4,6,16−18] Thus, attempts were made to hydrolyze the chlorogermane ClGe(O^{t}Bu)$_3$,[19] to obtain HOGe(O^{t}Bu)$_3$. However, reactions with water or various sources of hydroxide invariably gave a white, insoluble precipitate. This precipitate contained very small amounts of carbon and hydrogen and is therefore presumed to be (mostly) germanium oxide. Given these observations, attention turned to alternative titanium precursors with more stable germoxy ligands. Complex Ti[OGePh$_3$]$_4$, reported by Johnson and co-workers,[20,21] appeared to lack suitable solubility properties, and for this reason, the germoxy complex Ti[OGe^{i}Pr$_3$]$_4$ (**1**) was targeted.

The ligand precursor ^{i}Pr$_3$GeOH was prepared by a modification of the published procedure.[22] Hydrolysis of ^{i}Pr$_3$GeCl with NaOH (6 M) led to clean formation of ^{i}Pr$_3$GeOH, isolated in 85% yield after extraction from the aqueous solution. The homoleptic titanium complex **1** was prepared by two different routes, which involve reactions of ^{i}Pr$_3$GeOH (4 equiv) with Ti(O^{i}Pr)$_4$ in THF or with Ti(NMe$_2$)$_4$ in pentane (eq 1). Analytically pure colorless crystals of **1** were obtained by crystallization from a pentane solution at −30 °C. Notably, the analogous siloxide complex Ti[OSi^{i}Pr$_3$]$_4$ has previously been reported by Mansfeld and co-workers.[23] The ^{1}H nuclear magnetic resonance (NMR) spectrum of **1** in benzene-d_6 contains resonances at 1.34 and 1.56 ppm for the CH$_3$ and CH groups, respectively. Similarly, the solution ^{13}C NMR spectrum contains only two resonances, for the CH$_3$ (19.96 ppm) and CH (18.78 ppm) groups.

$$\begin{matrix}\mathrm{Ti(O^iPr)_4}\\ \text{or}\\ \mathrm{Ti(NMe_2)_4}\end{matrix} + 4\mathrm{HOGe^iPr_3} \xrightarrow[\text{or pentane},-4\mathrm{HNMe_2}]{\mathrm{THF},-4\mathrm{HO^iPr}} \underset{(\mathbf{1})}{\mathrm{Ti[OGe^iPr_3]_4}} \quad (1)$$

The bond connectivity of **1** was confirmed by X-ray crystallography. Although the diffraction data were not of sufficient quality to provide an accurate structural model, because of crystal twinning, the connectivity (Figure 1) in the molecule

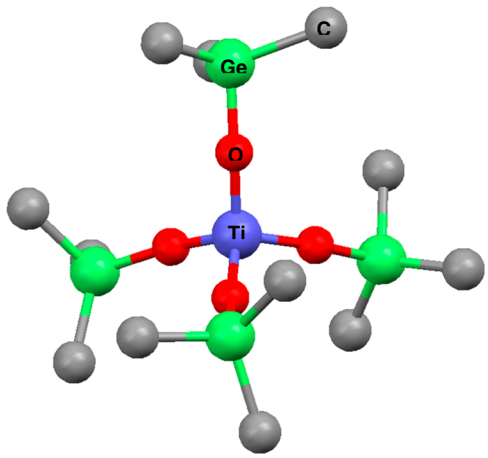

Figure 1. Connectivity of Ti[OGe^{i}Pr$_3$]$_4$ (**1**). Hydrogen atoms and isopropyl methyl groups have been omitted for the sake of clarity.

dx.doi.org/10.1021/cs400529x | ACS Catal. 2013, 3, 2269−2279

Scheme 2. Synthesis of $TiGe_3SBA15(x)$ and $TiGe_3SBA15(x)$-O_2 (a) or $TiSi_3SBA15$ and $TiSi_3SBA15$-O_2 (b)[a]

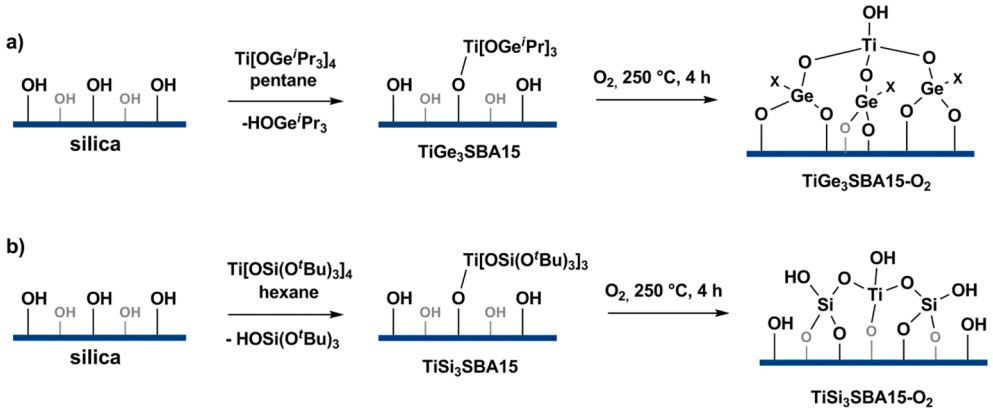

[a]The X substituent on Ge represents an oxygen- or carbon-based linkage (see the text).

was confirmed. The four covalently bound -OGe^{i}Pr$_3$ groups form an approximately tetrahedral coordination environment about the titanium center. Each germanium atom also exists in a roughly tetrahedral environment with one O−Ti bond and three -^{i}Pr ligands (Figure 1). This is similar to the related germanium complex Ti[OGePh$_3$]$_4$, reported by Johnson and co-workers,[21] as well as the siloxy analogues Ti[OSiPh$_3$]$_4$[21] and Ti-[OSiPh$_2$^{t}Bu]$_4$.[23]

The Fourier transform infrared (FTIR) spectrum of complex **1** exhibits a strong band at 804 cm^{-1} and a less intense band at 878 cm^{-1} assigned to two Ti−O−Ge stretching modes, by analogy with the previously reported complex Ti[OGePh$_3$]$_4$.[24] The UV−visible spectrum of **1** in a solution of hexanes (Figure S1 of the Supporting Information) displayed an intense absorption centered at a λ_{max} of 239 nm. This is presumably due to a ligand-to-metal charge transfer (LMCT) from the oxygen atoms to the titanium center.[25−27] This band is broadened and red-shifted with respect to analogous bands observed for the tetrahedral Ti(IV) complexes Ti[OSi(O^{t}Bu)$_3$]$_4$ (**2**, 227 nm)[17,18] and [(^{t}BuO)$_2$Ti(μ-O$_2$Si[OSi(O^{t}Bu)$_3$]$_2$)]$_2$ (216 nm).[17] No separate band for germanium is observed in the solution-state spectrum. It is possible that the single band observed for **1** contains contributions from both the O → Ti LMCT and absorptions due to the germanium centers. However, the solid-state diffuse-reflectance ultraviolet−visible (DRUV−visible) spectrum of **1** displayed two distinct absorptions at λ_{max} values of 223 and 261 nm. The former is likely due to the previously mentioned O → Ti LMCT, while the latter lies in the region of germanium absorption observed in doped sodalite powders[28] and mesoporous silica treated with germanium,[8] as well as for ^{i}Pr$_3$GeOH (Figure S1b of the Supporting Information, trace b).

The thermal decomposition behavior of **1** was examined by thermogravimetric analysis (TGA). The TGA trace of **1** under nitrogen (Figure S2 of the Supporting Information) reveals a precipitous weight loss occurring at ∼300 °C (heating rate of 10 °C/min). After the sample had been heated to 1000 °C, a ceramic yield of 2.5% was observed. This low ceramic yield is presumed to result from the sublimation of **1** and/or its decomposition products. The TGA trace of **1** under flowing oxygen also corresponds to a sharp weight loss but with a lower onset temperature (200 °C). In this case, the ceramic yield at 1000 °C was 31.2%, which is close to the value expected for TiO$_2$·2GeO$_2$ (31.4%).

Synthesis and Characterization of Supported Ti(IV) Catalysts. The mesoporous SBA15 silica was synthesized according to the literature procedure.[29] **$TiSi_3$SBA15** (0.18 wt % Ti) was prepared by methods previously described by grafting Ti[OSi(O^{t}Bu)$_3$]$_4$ (**2**) onto the silica surface to yield **$TiSi_3$SBA15**.[16,30] Analogously, **$TiGe_3$SBA15** materials were synthesized by the method outlined in Scheme 2. The maximal loading of titanium, measured by an inductively coupled plasma (ICP) method, was determined by employing a large excess of the precursor in reaction with SBA15. The maximal titanium loading for the **$TiGe_3$SBA15** materials is 3.59 wt % Ti, as measured by ICP. The initial grafting process was followed by ^{1}H NMR spectroscopy, and this showed that the sole elimination product of the grafting of complex **1** was ^{i}Pr$_3$GeOH. Monitoring this elimination product by ^{1}H NMR spectra, in the presence of a ferrocene internal standard, indicated that 1.0 equiv of ^{i}Pr$_3$GeOH was released per grafted molecule of complex **1**. This was also confirmed by the ratio of three germanium atoms per titanium atom on the surface, as measured by ICP (Table 1). In addition, a combustion analysis of **$TiGe_3$SBA15(1.5)** (with a Ti loading of 1.5 wt %) provided carbon (10.7%) and hydrogen (2.18%) contents consistent with the presence of surface-bound -OTi-[OGe^{i}Pr$_3$]$_3$ groups at a coverage of 0.45 nm^{-2}.

Table 1. Elemental Analysis and Nitrogen Physisorption Data for Dispersed Ti(IV) Materials

material	Ti content (wt %)[a]	Ge content (wt %)[a]	Ge/Ti (mol/mol)	S_{BET} (m^2/g)	r_p[b] (nm)
SBA15	–	–	–	840	3.9
$TiSi_3$SBA15	0.18	–	–	460	3.9
$TiSi_3$SBA15-O_2	0.19	–	–	470	3.9
$TiGe_3$SBA15(0.2)	0.21	0.92	3.1	470	3.9
$TiGe_3$SBA15(0.4)	0.41	1.99	3.2	440	3.9
$TiGe_3$SBA15(0.8)	0.75	3.61	3.2	420	3.3
$TiGe_3$SBA15(1.1)	1.10	4.81	2.9	410	3.3
$TiGe_3$SBA15(3.6)	3.59	–[c]	–[c]	230	3.3
$TiGe_3$SBA15(0.2)-O_2	0.24	1.2	3.2	570	3.9
$TiGe_3$SBA15(0.4)-O_2	0.44	2.0	3.1	560	3.9
$TiGe_3$SBA15(0.8)-O_2	0.86	4.3	3.3	550	3.9
$TiGe_3$SBA15(1.1)-O_2	1.19	6.3	3.4	530	3.9

[a]Determined by inductively coupled plasma (ICP) methods. [b]Pore radius measured by BJH adsorption. [c]Not determined.

Some of the **$TiGe_3$SBA15(x)** samples (where x corresponds to the weight percent of titanium) were treated at 250 °C (5 °C/min) for 4 h in flowing oxygen and then dried under vacuum for

dx.doi.org/10.1021/cs400529x | ACS Catal. 2013, 3, 2269−2279

12 h at 120 °C, to give samples designated as **TiGe$_3$SBA15(x)-O$_2$** (Scheme 2). This calcination temperature was chosen because it exceeds the observed onset temperature for thermolysis under oxygen (200 °C) but is below 300 °C to avoid agglomeration of titanium species, thus not yielding a well-defined single-site catalyst. After this calcination, the presence of residual carbon and hydrogen indicated that not all of the organic material was removed under these conditions. For **TiGe$_3$SBA15(1.5)-O$_2$**, the C (3.80%) and H (0.82%) analysis is consistent with the presence of (on average) one ^{i}Pr group per Ge, but the nature of this organic material remains unknown.

Nitrogen adsorption−desorption isotherms were used to measure the surface area and pore structure of the materials. All samples displayed N_2 adsorption−desorption data consistent with type IV isotherms (Figures S3 and S4 of the Supporting Information), with narrow pore size distributions, characteristic of SBA15-type materials.[29] The surface area of the materials decreased when a titanium-containing precursor was grafted to the surface, with **TiSi$_3$SBA15** displaying a Brunauer−Emmett−Teller (BET) surface area of 460 m^2/g and **TiGe$_3$SBA15** displaying a maximal surface area of 470 m^2/g (0.21 wt % sample), which decreased to a minimum of 410 m^2/g [1.1 wt % sample (Table 1)]. The 3.6 wt % sample displayed a much smaller hysteresis loop than samples with lower weight loadings (Figure S4f of the Supporting Information), along with a dramatically reduced surface area (230 m^2/g). After calcination, the **TiGe$_3$SBA15(x)-O$_2$** samples display an increase in surface area [530 m^2/g for **TiGe$_3$SBA15(1.1)-O$_2$** to 570 m^2/g for **TiGe$_3$SBA15(0.2)-O$_2$**]. This is probably due to removal of organic components of the molecular precursor, which leads to a greater nitrogen adsorption capacity. Transmission electron microscopy (TEM) confirmed that the well-ordered mesoporous structure of the materials was retained, even at the highest metal precursor loading (Figure S5 of the Supporting Information). This was corroborated by the retention of the low-angle reflections in the small-angle X-ray scattering patterns (Figures S6 and S7 of the Supporting Information).

DRUV−vis spectroscopy was used to probe the local coordination environment of the supported titanium(IV) catalysts. The DRUV−vis spectra of the supported catalysts **TiSi$_3$SBA15** and **TiGe$_3$SBA15(0.2)** are presented in Figure 2. These spectra feature an intense UV absorption band centered between 215 and 220 nm, due to the previously mentioned O → Ti LMCT band, similar in shape to the bands observed for **1** and **2** in solution. In spectra of **TiGe$_3$SBA15(x)** samples (Figure S8A of the Supporting Information), the intensity of this absorption increased with titanium loading, while the absorption maximum simultaneously shifted to a slightly lower energy (from 215 nm for 0.2 wt % Ti to 219 nm for 3.6 wt % Ti). Spectra of **TiGe$_3$SBA15(x)** also exhibit a shoulder centered at 250 nm that appears to be associated with the presence of germanium (*vide supra*) and is more prevalent in samples containing larger amounts of titanium and germanium. The similarity of spectra for the calcined **TiGe$_3$SBA15(x)-O$_2$** samples (Figure S8B of the Supporting Information) suggests that the Ti−O−Ge bonds are maintained after treatment with oxygen at 250 °C. Attempts to observe a vibration for the Ti−O−Ge linkages on the surface were not successful, presumably because of overlap with the intense Si−O−Si stretching mode of SBA15.

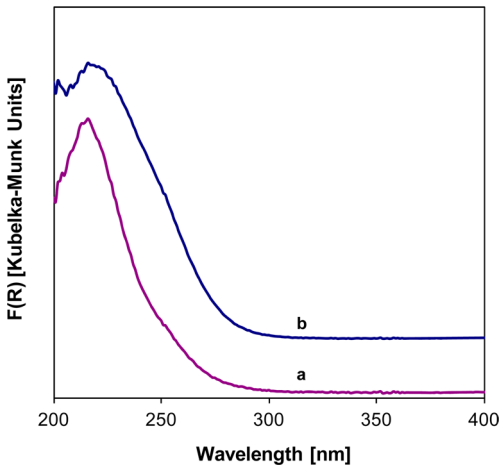

Figure 2. DRUV−vis spectra for (a) **TiSi$_3$SBA15** and (b) **TiGe$_3$SBA15(0.2)**. Spectra are offset for the sake of clarity.

XAS was also used to investigate the structures of **TiGe$_3$SBA15(0.25)** and **TiGe$_3$SBA15(0.25)-O$_2$** along with reference compounds, including Ti[OGe^{i}Pr$_3$]$_4$ (**1**). For the XAS studies, **TiGe$_3$SBA15(0.25)** and **TiGe$_3$SBA15(0.25)-O$_2$** were prepared by calcination at 300 °C for 1 h under a 20% O_2/He mixture. Figure 3A displays the normalized Ti K-edge XANES spectra for reference compounds Ti[OSi(O^{t}Bu)$_3$]$_4$ (**2**) and Ti(O^{i}Pr)$_4$ along with complex **1**, **TiGe$_3$SBA15(0.25)**, and **TiGe$_3$SBA15(0.25)-O$_2$**. Each compound displays a pre-edge peak at ∼4970 eV. The pre-edge peak parameters determined by fitting the pre-edge peaks with a Lorentzian function are listed in Table S1 of the Supporting Information. The molecular structures exhibit pre-edge peak heights and positions that are characteristic of Ti tetrahedrally coordinated by O. This was determined by comparison with the experimental data of Farges et al.[31] Differences in the pre-edge peak height of the molecular Ti complexes may be ascribed to imperfect tetrahedral structures, because perfect tetrahedral symmetry around the Ti center results in an intense pre-edge peak.[32] The symmetry of the Ti−O tetrahedron increases in the order Ti(O^{i}Pr)$_4$ < **1** < **2** based on the pre-edge peak heights compiled in Table S1 of the Supporting Information. Complex **1** exhibits an additional pre-edge peak at 4974 eV, similar to that observed for the homoleptic complex Ti[OGePh$_3$]$_4$.[13] During the grafting process, the pre-edge peak height decreases from a normalized peak height of 0.75 in **1** to 0.56 in **TiGe$_3$SBA15(0.25)**. This is likely a result of distortion of the near-perfect tetrahedral Ti−O coordination in the solid-state complex upon grafting, and loss of a single -OGe^{i}Pr$_3$ ligand. After oxygen treatment, the pre-edge peak height decreases further to 0.36 in **TiGe$_3$SBA15(0.25)-O$_2$**. Additionally, the peak position shifts to a slightly higher energy. These results suggest that the structure is distorted further away from a perfect tetrahedron during oxygen treatment. Similar behavior has been observed for tetrahedral Ti centers that have been exposed to water, which results in a decrease in peak height and a shift in peak position to a higher energy.[33−35] The decrease in pre-edge peak height and the shift to a higher energy are often ascribed to an increase in the level of coordination of the Ti center and is consistent with a mixture of 4- and 6-fold coordinated Ti.[31] Ti K-edge k^3-weighted *R*-space EXAFS spectra for **1**, **TiGe$_3$SBA15(0.25)**, and **TiGe$_3$SBA15(0.25)-O$_2$** are shown in Figure 3B. The fits for each of the EXAFS spectra are the dashed lines overlaid in Figure 3B. The results of EXAFS modeling are displayed in Table S2 of the Supporting Information. Complex **1** was fit by taking into account Ti−O first-shell scattering and Ti−O−Ge second-shell scattering. **TiGe$_3$SBA15(0.25)** and **TiGe$_3$SBA15(0.25)-O$_2$** were fit only in the first shell. All attempts to fit the second

dx.doi.org/10.1021/cs400529x | *ACS Catal.* 2013, 3, 2269−2279

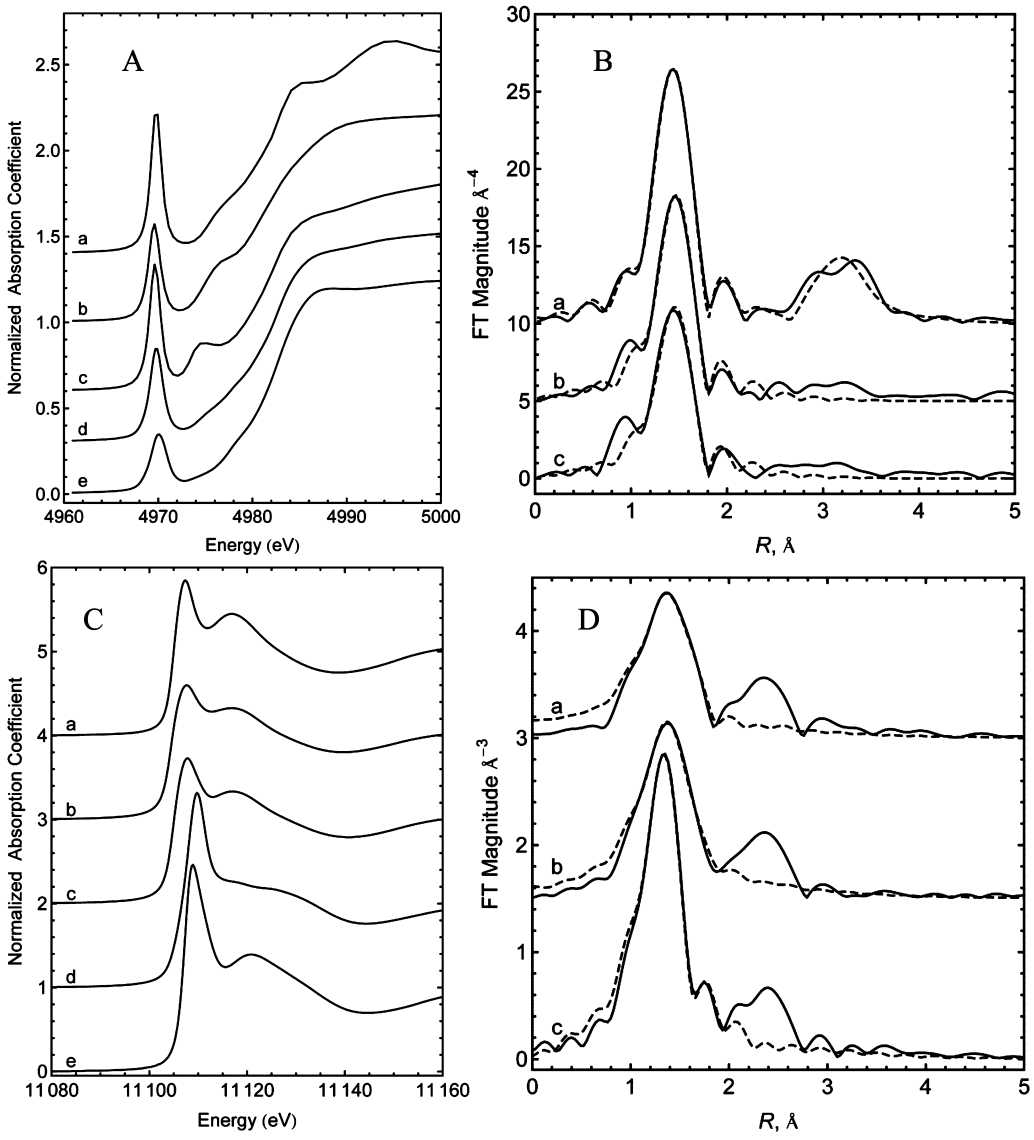

Figure 3. (A) Normalized experimental Ti K-edge XANES spectra for (a) Ti[OSi(O^{t}Bu)$_3$]$_4$, (b) Ti(O^{i}Pr)$_4$, (c) Ti[OGe^{i}Pr$_3$]$_4$ **1**, (d) **TiGe$_3$SBA15(0.25)**, and (e) **TiGe$_3$SBA15(0.25)-O$_2$**. Energy calibration was performed by setting the first inflection point of a reference Ti foil to 4966 eV. (B) Ti K-edge k^3-weighted *R*-space EXAFS spectra for (a) Ti[OGe^{i}Pr$_3$]$_4$ **1**, (b) **TiGe$_3$SBA15(0.25)**, and (c) **TiGe$_3$SBA15(0.25)-O$_2$**. Solid lines represent experimental data, and dashed lines are the corresponding fits. (C) Normalized experimental Ge K-edge XANES spectra for (a) ^{i}Pr$_3$GeOH, (b) Ti[OGe^{i}Pr$_3$]$_4$ **1**, (c) **TiGe$_4$SBA15(0.25)**, (d) **TiGe$_3$SBA15(0.25)-O$_2$**, and (e) Ge(OCH$_3$)$_4$. Energy calibration was performed by setting the first inflection point of a reference Ge$_{33}$Se$_{67}$ foil to 11103 eV. (D) Ge K-edge k^2-weighted *R*-space EXAFS spectra for (a) Ti[OGe^{i}Pr$_3$]$_4$ **1**, (b) **TiGe$_3$SBA15(0.25)**, and (c) **TiGe$_3$SBA15(0.25)-O$_2$**. Solid lines represent experimental data, and dashed lines are the corresponding fits. The spectra are artificially offset for the sake of clarity in all panels.

coordination shell of the grafted and calcined samples were unsuccessful because of minimal contributions to the *R*-space spectra in the region of ∼3 Å. An increase in the level of disorder in the second shell of the grafted and calcined samples would be consistent with the observed decrease in the *R*-space spectra in the region of ∼3 Å.

The Ge K-edge XANES spectra for ^{i}Pr$_3$GeOH, **1**, **TiGe$_3$SBA15(0.25)**, **TiGe$_3$SBA15(0.25)-O$_2$**, and Ge(OCH$_3$)$_4$ are shown in Figure 3C. The edge positions and white line heights extracted from these spectra are listed in Table S3 of the Supporting Information. **TiGe$_3$SBA15(0.25)** is very similar to **1** and ^{i}Pr$_3$GeOH in terms of edge position and white line height. This result suggests that Ge retains three C and one O nearest neighbors during the grafting process. During calcination, the edge position shifts from 11104.9 to 11108.1 eV and the white line height increases from 1.73 to 2.32 going from **TiGe$_3$SBA15(0.25)** to **TiGe$_3$SBA15(0.25)-O$_2$**, respectively. A shift in the edge position to higher energies suggests that Ge is bound to more electronegative elements after oxygen treatment. This is consistent with an increase in the Ge−O coordination level and a decrease in the Ge−C coordination level. **TiGe$_3$SBA15(0.25)-O$_2$** exhibits a XANES spectrum similar to that of Ge(OCH$_3$)$_4$. The experimental Ge K-edge EXAFS spectra are shown in Figure 3D (solid lines) along with the first-shell fits (dashed lines) only because all attempts to determine the structure of the second shell after calcination were unsuccessful. The fit parameters are listed in Table S4 of the Supporting Information. The coordination of Ge atoms shows little change from the solid-state complex to the grafted sample **TiGe$_3$SBA15(0.25)** as evidenced by the similarity in the EXAFS spectra and fit

dx.doi.org/10.1021/cs400529x | *ACS Catal.* 2013, 3, 2269−2279

parameters. During the oxygen treatment, the level of Ge−O coordination increases to 3.2 while the level of Ge−C coordination decreases to 0.8. This result is consistent with the findings of the Ge K-edge XANES. Calcination also leads to an increase in the EXAFS Debye−Waller factor from 2.5×10^{-3} to 3.8×10^{-3}. From these data, it appears that this oxygen treatment (20% O_2 for 1 h at 300 °C) does not remove all the organic material from Ge, as noted above, and is consistent with the presence of (on average) approximately one Ge−C linkage per Ge center.

Analysis of the Ti K-edge and Ge K-edge XANES and EXAFS suggests that upon grafting, the coordination environment around Ti changes from a perfect tetrahedron to a distorted tetrahedron, and the local coordination of Ge is unchanged. During calcination, there is a loss of Ge−C linkages that are mostly replaced by Ge−O bonds.

Catalytic Olefin Epoxidation. In control experiments with an oxidant and without a catalyst, or with a catalyst and no oxidant, no oxidation products of cyclohexene or 1-octene were detected by gas chromatography (GC) analysis. All titanium(IV)-containing samples are active olefin epoxidation catalysts with both *tert*-butyl hydroperoxide (TBHP) and cumene hydroperoxide (CHP) oxidants, as determined by GC analysis using dodecane as an internal standard. To determine whether any titanium species leached into solution during catalytic reactions, a sample of **TiGe$_3$SBA15(0.2)** was hot-filtered after reaction for 1 h, and the catalyst was recovered. The filtrate was kept at reaction temperature (65 °C) for 24 h. Aliquots taken from this mixture contained increasing amounts of oxidation products up to 1 h. Thereafter, the amounts of oxidation products remained constant for a 24 h reaction period. An identical reaction mixture that was not filtered exhibited increased amounts of oxidation products as the reaction progressed (Figure S9 of the Supporting Information). Additionally, recovered catalysts contained concentrations of titanium and germanium (measured by ICP methods) comparable to those of the corresponding materials prior to catalytic reactions.

Figure 4A describes the catalytic properties associated with **TiSi$_3$SBA15** and **TiGe$_3$SBA15(0.2)**, which possess a similar amount of Ti, for the reaction of cyclohexene with TBHP. These activities are represented by curves illustrating the turnover number (TON, defined as the moles of oxidation products produced per mole of titanium) as a function of time. The sample synthesized using the germanium precursor exhibits catalytic turnover numbers 50−150% greater than that of the silicon-containing catalyst at all times, with larger differences at shorter times. When the oxidant was changed from TBHP to CHP, after 9 h, the oxidation reaction became much more efficient for the **TiGe$_3$SBA15(0.2)** catalyst (with a 40% increase in the yield of oxidation products), while the **TiSi$_3$SBA15** catalyst gave approximately the same results (panel B vs panel A of Figure 4). With CHP as the oxidant for cyclohexene epoxidation, **TiGe$_3$SBA15(0.2)** displayed a 130% increase in the level of catalytic turnover compared to that of **TiSi$_3$SBA15** (Figure 4B). This notable increase in activity remained constant over the 9 h reaction, with a negligible change in selectivity [<2% higher (Figure S10b of the Supporting Information)].

The activities of all **TiGe$_3$SBA15(x)** catalysts in the epoxidation of cyclohexene with CHP are presented in Figure 5A. As the titanium content in the catalyst increases, the yield of cyclohexene oxide increases (Figure 5A,B). The selectivity for cyclohexene oxide was greater than 98% at all times for all catalysts. It should be noted that the maximal yield of

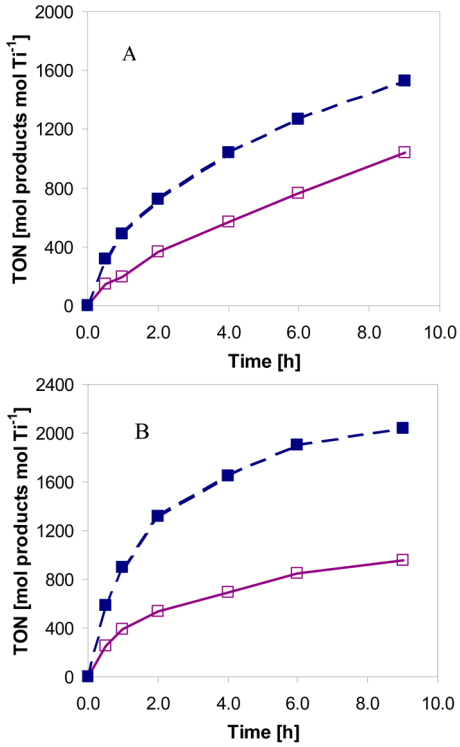

Figure 4. (A) Catalytic turnover number (TON) as a function of time during cyclohexene oxidation reactions with TBHP for **TiSi$_3$SBA15** (□) and **TiGe$_3$SBA15(0.2)** (■). (B) TON as a function of time during cyclohexene oxidation reactions with CHP for **TiSi$_3$SBA15** (□) and **TiGe$_3$SBA15(0.2)** (■). TON is defined as the moles of cyclohexene oxidation products per mole of titanium(IV).

cyclohexene oxide is 6.1 mmol [TON_{max} of 3650 for **TiGe$_3$SBA15(0.2)**], because CHP is the limiting reagent, and the curves begin to level off due to depletion of the reactant.

Interestingly, in contrast to cyclohexene epoxidation, epoxidation of the terminal olefin 1-octene is more efficient with TBHP as the oxidant. This can be seen for the catalyst derived from complex **1**, which exhibited significant increases in activity during catalytic 1-octene epoxidation reactions with TBHP as the oxidant (Figure 6). The catalyst **TiGe$_3$SBA15(0.2)** exhibited a 100−170% increase in catalytic activity with respect to that of **TiSi$_3$SBA15** after reaction for 9 h. This reaction was very efficient and selective, with both catalysts displaying high selectivity for the epoxide product, 1,2-epoxyoctane (>80% at all times). These catalysts continued to perform after reaction for 24 h, and when an additional aliquot of oxidant was added, the germanium-containing sample displayed 60% more activity (62 turnovers 6 h after additional oxidant added) than the silicon-containing catalyst (38 turnovers 6 h after additional oxidant added). The highest-weight loading catalyst tested in epoxidation reactions, **TiGe$_3$SBA15(1.1)**, displayed the highest yield of 1,2-epoxyoctane but exhibited catalytic turnover numbers comparable to those of **TiSi$_3$SBA15** (Figure 6).

With the calcined catalysts, the same trends were observed for the oxidation of cyclohexene. Overall, **TiGe$_3$SBA15(0.2)-O$_2$** displays a degree of conversion of cyclohexene that is 20% higher with CHP [vs TBHP (Figure S11 of the Supporting Information)]. In comparison to that of **TiSi$_3$SBA15(0.2)-O$_2$**, a 260% increase in the yield of cyclohexene oxide was observed for **TiGe$_3$SBA15(0.2)-O$_2$** (Figure 7). This remarkable increase in the level of formation of the cyclohexene oxide is also

dx.doi.org/10.1021/cs400529x | *ACS Catal.* 2013, 3, 2269−2279

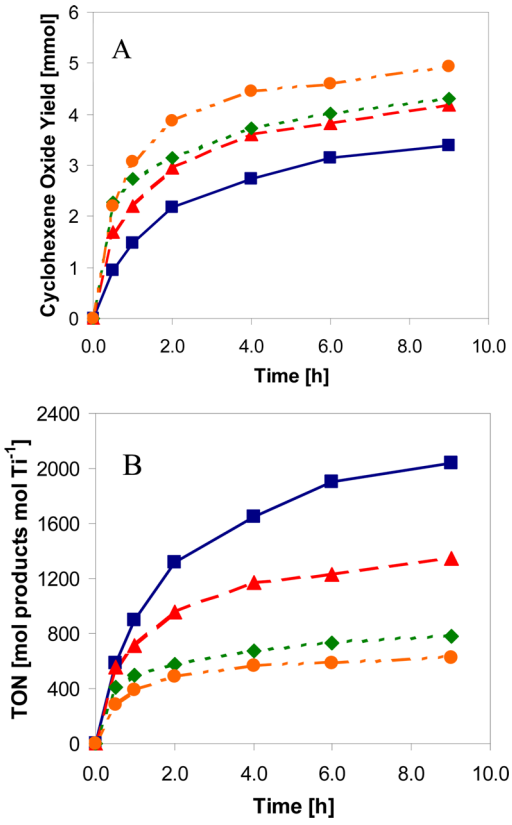

Figure 5. (A) Yield of cyclohexene oxide as a function of time for **TiGe$_3$SBA15(0.2)** (■), **TiGe$_3$SBA15(0.4)** (▲), **TiGe$_3$SBA15(0.8)** (◆), and **TiGe$_3$SBA15(1.1)** (●). (B) Catalytic turnover number (TON) as a function of time during cyclohexene oxidation reactions with CHP for **TiGe$_3$SBA15(0.2)** (■), **TiGe$_3$SBA15(0.4)** (▲), **TiGe$_3$SBA15(0.8)** (◆), and **TiGe$_3$SBA15(1.1)** (●). TON is defined as the moles of cyclohexene oxidation product per mole of titanium(IV). The selectivity to cyclohexene oxide was greater than 98% at all times.

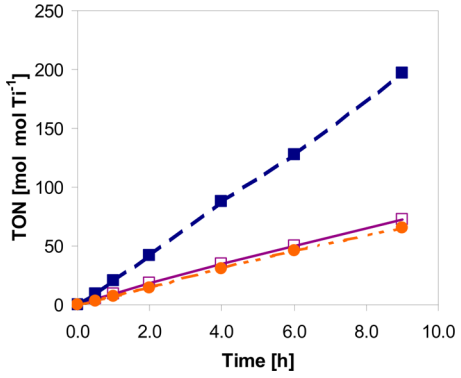

Figure 6. Catalytic turnover number (TON) as a function of time during 1-octene oxidation reactions with TBHP for **TiSi$_3$SBA15** (□), **TiGe$_3$SBA15(0.2)** (■), and **TiGe$_3$SBA15(1.1)** (●). TON is defined as the moles of 1-octene oxidation products per mole of titanium(IV). The selectivity to 1,2-epoxyoctane remained above 80% at all times and above 90% after 2 h for all catalysts.

associated with a high selectivity (>99%) in favor of the epoxide at all times. The yields of cyclohexene oxide from the CHP oxidant and the **TiGe$_3$SBA15(x)-O$_2$** catalysts are between 70 and 80% (Figure 8). By comparison with Figure 5A, which displays the yields of cyclohexene oxide for the uncalcined **TiGe$_3$SBA15(x)** catalysts, it is striking that only at the lowest

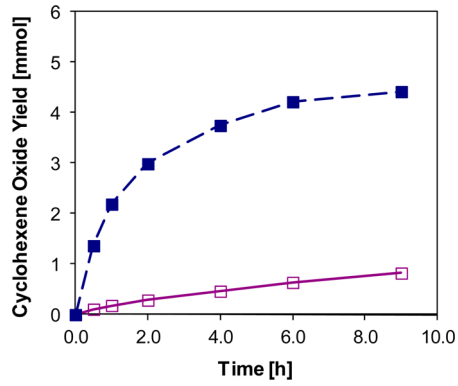

Figure 7. Yield of cyclohexene oxide as a function of time during cyclohexene oxidation with CHP for **TiSi$_3$SBA15-O$_2$** (□) and **TiGe$_3$SBA15(0.2)-O$_2$** (■).

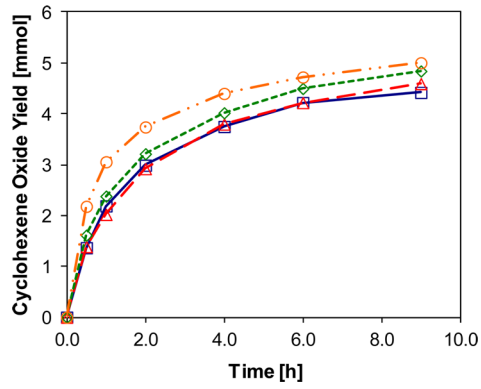

Figure 8. Yield of cyclohexene oxide as a function of time during cyclohexene oxidation reactions with CHP for **TiGe$_3$SBA15(0.2)-O$_2$** (□), **TiGe$_3$SBA15(0.4)-O$_2$** (△), **TiGe$_3$SBA15(0.8)-O$_2$** (◇), and **TiGe$_3$SBA15(1.1)-O$_2$** (○).

loading (0.18 wt % Ti) is there a significant difference between these catalysts in the conversion of the cyclohexene. Indeed, while **TiGe$_3$SBA15(x)** and **TiGe$_3$SBA15(x)-O$_2$** (x = 0.4, 0.8, and 1.1) display the same yield of cyclohexene oxide, an increase of 40% in the epoxide yield was observed for **TiGe$_3$SBA15(0.2)-O$_2$** (Figures 5A and 7). For the epoxidation of 1-octene, **TiGe$_3$SBA15(0.4)-O$_2$** displays a 65% increase in the 1,2-epoxyoctane yield (Figure S12 of the Supporting Information).

■ DISCUSSION

Synthesis and Characterization of Ti[OGe^{i}Pr$_3$]$_4$ (1) and TiGe$_3$SBA15 Materials. The nature of complex **1** was unambiguously determined by several spectroscopic techniques (NMR, UV−visible, and IR) and by X-ray crystallography. Thus, complex **1** features a tetrahedral titanium center and is useful as a spectroscopic model for tetrahedral Ti(IV)−germanium materials.

Reaction of complex **1** with the surface silanol groups of SBA15 anchors the Ti(IV) center to the silica surface, with liberation of 1 equiv of HOGe^{i}Pr$_3$. The XAS and DRUV−vis results confirm the presence of tetrahedral Ti(IV) centers after the grafting process and demonstrate that the coordination environment of Ge is unchanged. DRUV−vis spectra of all titanium-containing samples were dominated by an intense absorption between 215 and 220 nm. Bands in this region (200−220 nm) are indicative of titanium atoms in an isolated, tetrahedral environment.[25−27] No spectra of supported Ti(IV)

dx.doi.org/10.1021/cs400529x | ACS Catal. 2013, 3, 2269−2279

materials in this study exhibited bands due to larger oligomeric titanium domains (absorptions greater than 300 nm), such as titania (anatase, 330 nm).[26] The anhydrous conditions employed to synthesize these samples apparently prevent the formation of larger domains through the exclusion of water. These tetrahedral Ti(IV) sites are responsible for the observed catalytic activity, as already described well in the literature.[36−39] Spectra of **TiGe$_3$SBA15(x)** and **TiGe$_3$SBA15(x)-O$_2$** catalysts contained an additional band near 250 nm, the intensity of which increased with titanium loading. This band is presumably due to the presence of germanium in the samples, and not due to larger titanium oxide domains, because the DRUV−vis spectrum of complex **1** also exhibits a band in this region [λ_{max} = 261 nm (Figure 2)] and other germanium-containing materials display similar absorptions.[8,28] The fact that this band at 250 nm exists in both **TiGe$_3$SBA15(x)** and **TiGe$_3$SBA15(x)-O$_2$** suggests that even after calcination the structure around the Ti is maintained and the Ti−O−Ge linkage persists. XAS studies also confirm that during the grafting process, the tetrahedral environment about Ti is primarily maintained. Both XANES and EXAFS suggest that a single -OGe^{i}Pr$_3$ linkage is removed upon grafting, but this is difficult to quantify with EXAFS because of small contributions to the second shell of the *R*-space spectra. However, the pre-edge and XANES analyses are both consistent with the tetrahedral structure being slightly disrupted, which is consistent with the loss of one Ge-containing ligand and grafting of **1** to the SBA15 surface. Along with the loss of 1 equiv of HOGe^{i}Pr$_3$ (as determined by ^{1}H NMR spectroscopy), DRUV−vis and XAS data suggest a local environment for the Ti center on **TiGe$_3$SBA15** as represented in Scheme 1. After calcination, XANES/EXAFS analysis definitively showed that contributions from Ge−O coordination increase, which is consistent with the expectation for removal of the isopropyl group. The mesoporous framework of SBA15 is not significantly disturbed by the mild, low-temperature treatments used to prepare the samples in this study, as evidenced by retention of the low-angle reflections in the small-angle X-ray scattering patterns for all samples and the type IV isotherms observed.

Catalytic Performance. The improved performance of **TiGe$_3$SBA15(0.2)** relative to that of **TiSi$_3$SBA15** is consistent with reports of titanium supported on germanium-modified silica and homogeneous Ti(IV)−Ge catalysts for liquid-phase cyclohexene epoxidation,[11,13] as well as gold catalysts supported on germanium-doped titanosilicate-1 (TS-1) for the gas-phase epoxidation of propylene.[14] Theoretical calculations indicate that the germanium atom renders the titanium center and the transferred oxygen atom more electron-deficient, facilitating electrophilic oxygen transfer (presumably the kinetically relevant step for epoxidation).[14] It has to be noted that another precursor, Ti[OGePh$_3$]$_4$, was reported, along with its silicon analogue, Ti[OSiPh$_3$]$_4$, but only grafting and catalysis with the silicon compound were reported.[13,20,21]

The structure of the hydroperoxide oxidant plays a role in determining product selectivity and the rate of epoxidation.[11,40,41] An increased epoxidation efficiency was observed when using CHP in place of TBHP as the oxidant for both **TiSi$_3$SBA15** and **TiGe$_3$SBA15(0.2)**, in the epoxidation of cyclohexene. This is in agreement with previous work in our laboratory employing supported Ti(IV) catalysts,[16] but in contrast with reports of other Ti(IV) catalysts supported on mesoporous silica.[11] Thus, the catalysts described here represent an attractive alternative, given the much lower cost of CHP relative to TBHP. In contrast to previous reports of the epoxidation of allyl chloride[41] and cyclohexene,[11] the epoxide selectivity increased for both **TiSi$_3$SBA15** and **TiGe$_3$SBA15-(0.2)** catalysts when CHP was used as the oxidant instead of TBHP. The decreased activity observed with higher titanium loadings in **TiGe$_3$SBA15(x)** samples is consistent with other studies of silica-supported titanium(IV) catalysts.[16,27,42−45] This trend suggests that the most isolated titanium sites are more active, and catalysts with lower weight loadings possess a higher proportion of the most active sites. Relative to that of **TiSi$_3$SBA15**, catalysts synthesized from complex **1** with comparable titanium weight loadings [**TiGe$_3$SBA15(0.2)**] also exhibited increased activity in the epoxidation of 1-octene with TBHP. However, the higher-weight loading material, **TiGe$_3$SBA15(1.1)**, displayed a decreased catalytic turnover number compared to that of **TiGe$_3$SBA15(0.2)** (on a per titanium basis), consistent with the lower-weight loading sample containing a higher proportion of the isolated, more active titanium sites. All catalysts derived from Ti[OGe^{i}Pr$_3$]$_4$ (**1**) display approximately the same yield of cyclohexene oxide before and after treatment in oxygen at 250 °C, except **TiGe$_3$SBA15-(0.2)-O$_2$**, for which an increase of the cyclohexene yield of 40% was observed. These results are also consistent with the most isolated sites being the most active.

CONCLUSIONS

The preparation and structural characterization of a new germanium-containing titanium(IV) molecular precursor, Ti[OGe^{i}Pr$_3$]$_4$ (**1**), have been described. This compound is a useful model for tetrahedral titanium(IV) sites supported on germania and other metal oxides, and several spectroscopic techniques (NMR, FTIR, UV−vis, DRUV−vis spectroscopy, and XAS) have been employed to probe its structure. Use of this germoxy-containing compound in the thermolytic molecular precursor approach allows control over the environment of the surface-bound catalytic center. The grafting chemistry of complex **1** is very clean, such that upon reaction with surface silanol sites in mesoporous silica, one germoxide ligand is displaced (as HOGe^{i}Pr$_3$) to give a pseudotetrahedral mononuclear titanium(IV) species with three -OGe linkages and one -OSi$_{surface}$ linkage. Spectroscopic evidence suggests the environment of the titanium sites remains similar to that found for the solution-state precursor. This is, to the best of our knowledge, the first report of a germanium-containing titanium(IV) compound used to generate surface-bound metal sites for catalytic oxidation reactions. Moreover, treatment of grafted precursor **1** at 250 °C under oxygen led to an oxygenated environment around the germanium with removal of most (but not all) of the organic groups.

Supported catalysts derived from complex **1** were active in the epoxidation of both cyclohexene and 1-octene using alkyl hydroperoxides. These catalysts were at least 100% more efficient than catalysts synthesized from all-silicon-containing precursors for the epoxidation of cyclohexene with CHP or TBHP. It was determined that the most efficient oxidant for the epoxidation of cyclohexene was CHP, and that the catalyst with the lowest titanium content (0.21 wt %) contained the largest fraction of isolated, highly active Ti(IV) sites. Future work in this area will focus on the synthesis of new precursors containing fewer than four germanium-containing ligands to study the effect of multiple Ti−O−Ge linkages on catalytic epoxidation reactions. Moreover, previous reports from this laboratory have shown that supported tantalum catalysts,[5−7,40] including some postmodified with germanium,[8] display a better catalytic activity for

dx.doi.org/10.1021/cs400529x | ACS Catal. 2013, 3, 2269−2279

epoxidation than their titanium analogues when hydrogen peroxide is used as the oxidant. In this context, current work is focusing on the development of tantalum precursors possessing germanium in their coordination sphere and their use in epoxidation catalysis.

EXPERIMENTAL SECTION

General Procedures. All manipulations were conducted under an inert nitrogen atmosphere using standard Schlenk techniques or in a Vacuum Atmospheres drybox, unless otherwise noted. Dry, oxygen-free solvents were used throughout. Benzene-d_6 was purified and dried via vacuum distillation from a sodium/potassium alloy. Toluene was purchased from Aldrich and distilled over sodium prior to use. Cyclohexene was purchased from Aldrich and dried over CaH_2 prior to use. *tert*-Butyl hydroperoxide (TBHP, 5.5 M in decane), cumene hydroperoxide (CHP, 80%, technical grade), and $Ti(O^iPr)_4$ were purchased from Aldrich and used as received. Triisopropylchlorogermane was purchased from Gelest, Inc., and used without further purification. Mesoporous SBA15,[29] $(^tBuO)_3SiOH$,[46] $Ti[OSi(O^tBu)_3]_4$ **2**,[30] and $Mg(CH_2C_6H_5)_2\cdot 2THF$[47] were prepared as reported in the literature, dehydrated under dynamic vacuum, and stored in a Vacuum Atmospheres drybox until they were used.

Synthesis of ^{i}Pr$_3$GeOH. To pure ^{i}Pr$_3$GeCl (4.09 g, 17.2 mmol) was added an excess of aqueous NaOH (6 M, 16 mL, 96 mmol, 5.6 equiv). The mixture was stirred vigorously for 1 h at 50 °C and then allowed to settle. The organic layer was removed, and the aqueous layer was extracted three times with 15 mL of hexanes. The solution of hexanes was dried over $MgSO_4$ and filtered on a Büchner funnel. The solvent was removed *in vacuo* and afforded **1** as a colorless oil in 82% yield (3.09 g, 14.1 mmol): ^{1}H NMR (C_6D_6, 400 MHz) δ −0.04 (s, 1H, O*H*), 1.09 (d, J_{HH} = 7.2 Hz, 18H, CH_3), 1.25 (sept, J_{HH} = 7.3 Hz, 3H, C*H*); ^{13}C(^{1}H) NMR δ 17.21 (*C*H), 19.33 (*C*H_3). Anal. Calcd for $C_9H_{22}GeO$: C, 49.38; H, 10.12. Found: C, 49.46; H, 10.35.

Synthesis of Ti[OGe^{i}Pr$_3$]$_4$ (1). *Method A.* This compound was prepared by adapting the preparation of silicon analogue $Ti[OSi^iPr_3]_4$, reported by Mansfeld and co-workers. To a solution of $Ti(O^iPr)_4$ (0.307 g, 1.08 mmol) in THF was added a solution of ^{i}Pr$_3$GeOH (0.969 g, 4.43 mmol, 4.1 equiv) in THF. The mixture was stirred for 18 h at room temperature, and the solvent was removed *in vacuo* at 40 °C, leaving a colorless solid (86% yield, 0.854 g, 0.93 mmol).

Method B. To a solution of $Ti(NMe_2)_4$ (0.087 g, 0.383 mmol) in pentane was added a solution of ^{i}Pr$_3$GeOH (0.340 g, 1.55 mmol, 4.0 equiv) in pentane. The mixture was stirred for 4 h at room temperature, and the solvent was removed in vacuo at 40 °C, leaving a colorless solid. Analytically pure colorless and suitable crystals for X-ray crystallography (85% yield, 0.300 g, 0.326 mmol) were obtained by crystallization from a pentane solution at −30 °C: ^{1}H NMR (C_6D_6, 300 MHz) δ 1.56 (sept, J_{HH} = 7.4 Hz, 3H, C*H*), 1.34 (d, J_{HH} = 7.2 Hz, 18H, CH_3); ^{13}C(^{1}H) NMR δ 18.78 (*C*H), 19.96 (*C*H_3). Anal. Calcd for $C_{36}H_{84}Ge_4O_4Ti$: C, 47.02; H, 9.21. Found: C, 46.97; H, 9.14.

X-ray Crystallography. The X-ray analysis of complex **1** was conducted at the University of California, Berkeley, CHEXRAY crystallographic facility. Measurements were taken on an APEX-II CCD area detector with a HELIOS multilayer mirror monochromating device using Cu Kα radiation (λ = 1.54184 Å). Data were integrated, and empirical absorption corrections were made using the APEX2 program package. The structure was determined by direct methods and expanded using Fourier techniques. All calculations were performed using the SHELXTL crystallographic package.

Synthesis of TiGe$_3$SBA15(x), TiSi$_3$SBA15, TiGe$_3$SBA15-(x)-O$_2$, and TiSi$_3$SBA15-O$_2$. A sample of SBA15 was dried at 120 °C under vacuum for 16 h and handled under a nitrogen atmosphere. A 0.7 g sample of SBA15 was suspended in hexanes (40 mL). A 20 mL solution of $Ti[OGe^iPr_3]_4$ (**1**) (0.039−0.201 g, 0.036−0.223 mmol) or $Ti[OSi(O^tBu)_3]_4$ (**2**) (0.036 g, 0.039 mmol) in hexanes was added via cannula at 25 °C while the samples were being vigorously stirred. The resulting mixture was stirred for 18 h, filtered via cannula, and rinsed with hexanes (3 × 50 mL). The filtered material was dried under vacuum for 2 h at 25 °C and subsequently for 12 h at 120 °C to give **TiGe$_3$SBA15(x)** (where x is the weight percent of Ti) and **TiSi$_3$SBA15**, respectively. A portion of these materials was treated at 250 °C (5 °C/min) for 4 h in flowing oxygen and subsequently dried again for 12 h at 120 °C. The resulting materials are designated **TiGe$_3$SBA15(x)-O$_2$** and **TiSi$_3$SBA15-O$_2$**, respectively.

Characterization. Solution NMR spectra were recorded at 400 MHz using a Bruker AVQ-400, AV-300 spectrometer (^{1}H, ^{13}C). Nitrogen adsorption measurements were taken using a Quantichrome Autosorb 1 instrument, and samples were outgassed for 12 h at 120 °C prior to measurement. Infrared spectra were recorded using a Thermo Nicolet 6700 FTIR spectrometer. Elemental analyses were performed using a Perkin-Elmer Optima 7000 DV optical emission spectrometer at the University of California, Berkeley, College of Chemistry Elemental Analysis Facility. Small-angle X-ray scattering experiments were performed with a Bruker Nanostar spectrometer, using a copper tube as the X-ray source (Cu Kα radiation). UV−vis spectra were recorded using a Varian-Cary 300 Bio spectrophotometer. DRUV−vis spectra were recorded using the same spectrophotometer with a diffuse-reflectance attachment. MgO was used as the 100% transmittance standard. Thermal gravimetric analyses were performed with a Seiko Instruments Inc. EXSTAR 6000 TG/DTA 6300 instrument under a 100 cm^3/min flow of nitrogen or oxygen and a heating rate of 5 °C/min. The hydroxyl group content of samples was determined by reaction with $Mg(CH_2C_6H_5)_2\cdot 2THF$ and quantification of the evolved toluene via ^{1}H NMR spectroscopy. GC analyses were performed on an HP 6890N system using a phenyl methyl polysiloxane DB-5 capillary column (30.0 m × 320 μm × 1.00 μm), and integration was performed relative to a dodecane internal standard.

X-ray absorption measurements were performed at the X19A beamline of the National Synchrotron Light Source at Brookhaven National Laboratory (Upton, NY). Ti K-edge (4966 eV) and Ge K-edge (11103 eV) EXAFS analyses were conducted in a He atmosphere at room temperature. Samples were prepared by spreading powder on a piece of polyimide tape. The tape was folded multiple times to achieve a uniform sample thickness. All data for the samples were collected in fluorescence geometry using a passivated implanted planar silicon (PIPS) detector. A reference Ti foil was used to calibrate the Ti K-edge X-ray energy at 4966 eV, and a reference $Ge_{33}Se_{67}$ foil was used to calibrate the Ge K-edge X-ray energy at 11103 eV for each spectrum. Reference foils were placed between the transmission ionization chamber and a reference ionization chamber. The IFEFFIT package was used to process and analyze the data.[48,49]

Catalytic Cyclohexene Epoxidation. A sample of catalyst (0.035 g) was added to a 25 mL round-bottom flask fitted with a reflux condenser and a septum. Under a flow of nitrogen, toluene

dx.doi.org/10.1021/cs400529x | ACS Catal. 2013, 3, 2269−2279

(5 mL) and cyclohexene (1.0 mL, 9.9 mmol) were added via syringe. Dodecane (50 μL) was added as an internal standard. The mixture was heated to 65 °C, where it was allowed to equilibrate for 15 min before the oxidant (1.1 mL or 6.05 mmol of TBHP, 5.5 M in decane, or 1.1 mL of 6.1 mmol of CHP, 80% technical grade) was added via syringe to the rapidly stirred solution. Aliquots (100 μL) were taken from the reaction mixture via syringe, filtered, and cooled. The filtrate was analyzed by gas chromatography (GC), and products were assigned on the basis of known samples analyzed under the same conditions.

Catalytic 1-Octene Epoxidation. A sample of catalyst (0.035 g) was added to a 25 mL round-bottom flask fitted with a reflux condenser and a septum. Under a flow of nitrogen, toluene (5 mL) and 1-octene (1.55 mL, 9.9 mmol) were added via syringe. Dodecane (50 μL) was added as an internal standard. The mixture was heated to 65 °C, where it was allowed to equilibrate for 15 min before the oxidant (1.1 mL or 6.05 mmol of TBHP, 5.5 M in decane, or 1.1 mL or 6.1 mmol of CHP, 80% technical grade) was added via syringe to the rapidly stirred solution. Aliquots (100 μL) were taken from the reaction mixture via syringe, filtered, and cooled. The filtrate was analyzed by GC, and products were assigned on the basis of known samples analyzed under the same conditions.

■ ASSOCIATED CONTENT

Supporting Information

Nitrogen adsorption−desorption isotherms and small-angle X-ray scattering patterns for SBA15 and all dispersed Ti catalysts, UV−vis and DRUV−vis spectra of **1** and **2**, TGA of **1**, additional DRUV−vis spectra of $\mathbf{TiGe_3SBA15}(x)$ and $\mathbf{TiGe_3SBA15}(x)\text{-}\mathbf{O_2}$, XAS parameters, and additional epoxide yields and selectivities. This material is available free of charge via the Internet at http://pubs.acs.org.

■ AUTHOR INFORMATION

Corresponding Author

*E-mail: tdtilley@berkeley.edu.

Notes

The authors declare no competing financial interest.

■ ACKNOWLEDGMENTS

We gratefully acknowledge the support of the Director, Office of Energy Research, Office of Basic Energy Sciences, Chemical Sciences Division, of the U.S. Department of Energy (DOE) under Contract DE-AC02-05CH11231. We thank Professor A. P. Alivisatos of the University of California, Berkeley, for the use of instrumentation (TEM and SAXS). We thank the Synchrotron Catalysis Consortium at the National Synchrotron Light Source at Brookhaven National Laboratory for their help in obtaining X-ray absorption data. Beamline X19A is supported, in part, by U.S. DOE Grant DE-FG02-05ER15688. C.S.S. acknowledges the support of the National Science Foundation through a Graduate Research Fellowship under Grant DGE-070756. R.M.R. acknowledges support from 3M through a Non-Tenured Faculty Grant (NTFG).

■ REFERENCES

(1) Tilley, T. D. *J. Mol. Catal. A: Chem.* **2002**, *182*, 17.
(2) Thomas, J. M.; Raja, R.; Lewis, D. W. *Angew. Chem., Int. Ed.* **2005**, *44*, 6456.
(3) Fujdala, K. L.; Tilley, T. D. *J. Catal.* **2003**, *216*, 265.
(4) Brutchey, R. L.; Ruddy, D. A.; Andersen, L. K.; Tilley, T. D. *Langmuir* **2005**, *21*, 9576.
(5) Ruddy, D. A.; Tilley, T. D. *Chem. Commun.* **2007**, 3350.
(6) Ruddy, D. A.; Brutchey, R. L.; Tilley, T. D. *Top. Catal.* **2008**, *48*, 99.
(7) Ruddy, D. A.; Tilley, T. D. *J. Am. Chem. Soc.* **2008**, *130*, 11088.
(8) Cordeiro, P. J.; Tilley, T. D. *Langmuir* **2011**, *27*, 6295.
(9) Cordeiro, P. J.; Tilley, T. D. *ACS Catal.* **2011**, *1*, 455.
(10) Oldroyd, R. D.; Thomas, J. M.; Sankar, G. *Chem. Commun.* **1997**, 2025.
(11) Oldroyd, R. D.; Sankar, G.; Thomas, J. M.; Ozkaya, D. *J. Phys. Chem. B* **1998**, *102*, 1849.
(12) Cimpeanu, V.; Parvulescu, V. I.; Amoros, P.; Beltran, D.; Thompson, J. M.; Hardacre, C. *Chem.—Eur. J.* **2004**, *10*, 4640.
(13) Thomas, J. M.; Sankar, G.; Klunduk, M. C.; Attfield, M. P.; Maschmeyer, T.; Johnson, B. F. G.; Bell, R. G. *J. Phys. Chem. B* **1999**, *103*, 8809.
(14) Liu, T.; Hacarlioglu, P.; Oyama, S. T.; Luo, M.-F.; Pan, X.-R.; Lu, J.-Q. *J. Catal.* **2009**, *267*, 202.
(15) Moliner, M.; Diaz-Cabanas, M. J.; Fornes, V.; Martinez, C.; Corma, A. *J. Catal.* **2008**, *254*, 101.
(16) Jarupatrakorn, J.; Tilley, J. D. *J. Am. Chem. Soc.* **2002**, *124*, 8380.
(17) Brutchey, R. L.; Mork, B. V.; Sirbuly, D. J.; Yang, P. D.; Tilley, T. D. *J. Mol. Catal. A: Chem.* **2005**, *238*, 1.
(18) Terry, K. W.; Tilley, T. D. *Chem. Mater.* **1991**, *3*, 1001.
(19) Pike, R. M.; Fournier, A. F. *Recl. Trav. Chim. Pays-Bas* **1962**, *81*, 475.
(20) Attfield, M. P.; Sankar, G.; Thomas, J. M. *Catal. Lett.* **2000**, *70*, 155.
(21) Johnson, B. F. G.; Klunduk, M. C.; Martin, C. M.; Sankar, G.; Teate, S. J.; Thomas, J. M. *J. Organomet. Chem.* **2000**, *596*, 221.
(22) Anderson, H. H. *J. Am. Chem. Soc.* **1953**, *75*, 814.
(23) Mansfeld, D.; Schurmann, M.; Mehring, M. *Appl. Organometal. Chem.* **2005**, *19*, 1185.
(24) Stepovik, L. P.; Gulenova, M. V. *Russ. J. Gen. Chem.* **2006**, *76*, 235.
(25) Blasco, T.; Corma, A.; Navarro, M. T.; Pariente, J. P. *J. Catal.* **1995**, *156*, 65.
(26) Klein, S.; Weckhuysen, B. M.; Martens, J. A.; Maier, W. F.; Jacobs, P. A. *J. Catal.* **1996**, *163*, 489.
(27) Marchese, L.; Maschmeyer, T.; Gianotti, E.; Coluccia, S.; Thomas, J. M. *J. Phys. Chem. B* **1997**, *101*, 8836.
(28) Todd, L. T.; Tranjan, F. M. *J. Electrochem. Soc.* **1980**, *127*, 435.
(29) Zhao, D. Y.; Huo, Q. S.; Feng, J. L.; Chmelka, B. F.; Stucky, G. D. *J. Am. Chem. Soc.* **1998**, *120*, 6024.
(30) Coles, M. P.; Lugmair, C. G.; Terry, K. W.; Tilley, T. D. *Chem. Mater.* **2000**, *12*, 122.
(31) Farges, F.; Brown, G. E.; Rehr, J. J. *Phys. Rev. B* **1997**, *56*, 1809.
(32) Babonneau, F.; Doeuff, S.; Leaustic, A.; Sanchez, C.; Cartier, C.; Verdaguer, M. *Inorg. Chem.* **1988**, *27*, 3166.
(33) Blasco, T.; Camblor, M. A.; Corma, A.; Esteve, P.; Guil, J. M.; Martinez, A.; Perdigon-Melon, J. A.; Valencia, S. *J. Phys. Chem. B* **1998**, *102*, 75.
(34) Notestein, J. M.; Andrini, L. R.; Kalchenko, V. I.; Requejo, F. G.; Katz, A.; Iglesia, E. *J. Am. Chem. Soc.* **2007**, *129*, 1122.
(35) Ikeue, K.; Yamashita, H.; Anpo, M.; Takewaki, T. *J. Phys. Chem. B* **2001**, *105*, 8350.
(36) Ikeue, K.; Ikeda, S.; Watanabe, A.; Ohtani, B. *Phys. Chem. Chem. Phys.* **2004**, *6*, 2523.
(37) Ward, A. J.; Lesic, R.; Masters, A. F.; Maschmeyer, T. *Proc. R. Soc. London, Ser. A* **2012**, *468*, 1968.
(38) Thomas, J. M. *Proc. R. Soc. London, Ser. A* **2012**, *468*, 1884.
(39) Che, M.; Mori, K.; Yamashita, H. *Proc. R. Soc. London, Ser. A* **2012**, *468*, 2113.
(40) Ledon, H. J.; Varescon, F. *Inorg. Chem.* **1984**, *23*, 2735.
(41) Sheldon, R. A.; Vandoorn, J. A.; Schram, C. W. A.; Dejong, A. J. *J. Catal.* **1973**, *31*, 438.
(42) Klunduk, M. C.; Maschmeyer, T.; Thomas, J. M.; Johnson, B. F. G. *Chem.—Eur. J.* **1999**, *5*, 1481.
(43) Oldroyd, R. D.; Thomas, J. M.; Maschmeyer, T.; MacFaul, P. A.; Snelgrove, D. W.; Ingold, K. U.; Wayner, D. D. M. *Angew. Chem., Int. Ed.* **1996**, *35*, 2787.

(44) Maschmeyer, T.; Rey, F.; Sankar, G.; Thomas, J. M. *Nature* **1995**, *378*, 159.
(45) Ferreira, P.; Goncalves, I. S.; Kuhn, F. E.; Pillinger, M.; Rocha, J.; Santos, A. M.; Thursfield, A. *Eur. J. Inorg. Chem.* **2000**, 551.
(46) Abe, Y.; Kijima, I. *Bull. Chem. Soc. Jpn.* **1969**, *42*, 1118.
(47) Dryden, N. H.; Legzdins, P.; Rettig, S. J.; Veltheer, J. E. *Organometallics* **1992**, *11*, 2583.
(48) Ravel, B.; Newville, M. *J. Synchrotron Radiat.* **2005**, *12*, 537.
(49) Newville, M. *J. Synchrotron Radiat.* **2001**, *8*, 322.